V. Dolejsi

Anisotropic Mesh Adaptation Technique for Viscous Flow Simulation

Preprint No. MATH-knm-2001/2

14.03.2001

Submitted to *East-West Journal of Numerical Mathematics*

Katedra numericke matematiky, Faculty of Mathematics and Physics,
Charles University, Sokolovská 83, 186 75 Praha 8, Czech Republic

*t*http://www.karlin.mff.cuni.cz/ms-preprints/

Cover print by Reprostedisko, Malostransk nm. 25, Praha 1 - Mal Strana
Design by Mirko Rokyta, picture of snowflake by Ondej Kalenda
Current series administrator: V. Dolejsi

Anisotropic Mesh Adaptation Technique for Viscous Flow Simulation

Vít Dolejší

Department of Numerical Mathematics
Faculty of Mathematics and Physics
Charles University
Sokolovská 83
186 00 Praha 8
Czech Republic

Abstract

We present an efficient adaptive method for unstructured triangular meshes especially developed for the numerical simulation of viscous compressible flow. This method uses the anisotropic mesh adaptation (AMA) technique introduced in [6], [9] with some additional improvement reflecting physical properties of viscous high speed flow. We summarize the AMA method with its geometrical interpretation and we describe the numerical solver, which uses the combination of finite volume and finite element methods. We show that the direct application of AMA technique is not suitable for the viscous flow simulation and we propose some modifications, namely for capturing boundary layers and a wake. Moreover an additional smoothing technique increasing the regularity of the triangulation is presented.

1 Introduction

We deal with the numerical solution of the Navier-Stokes equations describing the motion of viscous compressible flow. The quality of numerical solution strongly depends on the used meshes. The subject of this paper concerns the adaptation of unstructured triangular grids for finite element and/or finite volume methods. The general aim is to have a triangulation with as small as possible number of elements where the prescribed accuracy of the numerical solution is achieved.

During last years we have developed the *anisotropic mesh adaptation* (AMA) algorithm, which adapt a given triangulation to the new one, where better numerical solution can be achieved. We described AMA technique with implementation details in [6] and there the successful application for the simulation of **inviscid** transonic flow was presented. In [9] we have deeply developed the theoretical background of AMA and we have formulated its application for a numerical solution of a general boundary value problem (BVP). We have derived a *necessary condition* for a triangulation such that the given accuracy of the numerical solution is satisfied. Then we have shown, that under some assumptions, this necessary condition is fulfilled for triangulations generated by AMA.

Although the theoretical determination in [9] was independent of the considered problem, many numerical results show, that the direct application of AMA for **viscous** flow simulation brings some problems, namely in the capturing of boundary layers and wakes, especially for high speed flow with small viscosity. Therefore an additional mesh adaptation technique have to be included into the AMA algorithm. Here we propose an improvement of adaptive technique for the computation of viscous compressible flow. Except the necessary condition presented in [9] we include new artificial conditions, whose forms follow from the physical properties of viscous transonic flow. In Section 2 we summarize the results from [6] and [9] in the form suitable for further consideration. The governing equations describing the motion of viscous compressible flow and their discretization is presented in Section 3. Section 4 contains the extension of AMA for viscous flow simulation. Numerical examples and their comparison are presented in Section 5.

2 Summary of AMA technique

At the beginning of this section we briefly describe the AMA algorithm, which is in details presented in [6] and [9].

2.1 Necessary condition

Let us consider scalar boundary value problem (BVP) in the set Ω, where $\Omega \subset I\!R^2$ is a bounded domain. We introduce the weak formulation of (BVP): Find the function function $u : \Omega \to I\!R$ satisfying

$$u \in U, \tag{2.1}$$

$$\mathcal{L}(u, v) = f(v) \quad \forall v \in V, \tag{2.2}$$

$$\mathcal{B}(u) \in V. \tag{2.3}$$

here U and V are the trial and test function spaces, respectively, (2.2) represents the weak form of the partial differential equation under consideration and (2.3) guarantees, that the prescribed boundary conditions are fulfilled in the sense of traces. The function u satisfying (2.1) – (2.3) is called the *exact solution*. Let us suppose that the problem (2.1) – (2.3) has a unique exact solution.

We seek the numerical solution of (2.1) – (2.3) in the space of piecewise linear functions using a suitable numerical method, e.q. finite element method (FEM), finite volume method (FVM). To this end we replace the domain Ω by its polygonal approximation Ω_h and we construct the triangulation $\mathcal{T}_h$ of Ω_h with standard properties from FEM ([3], [10], [14]). The *approximate solution* of problem (2.1) – (2.3) is defined as a function $u_h : \overline{\Omega}_h \to I\!R$ satisfying

$$u_h \in U_h, \tag{2.4}$$

$$\mathcal{L}_h(u_h, v_h) = f_h(v_h) \quad \forall v_h \in V_h, \tag{2.5}$$

$$\mathcal{B}_h(u_h) \in V_h. \tag{2.6}$$

Here

$$U_h = \left\{ u_h \in L^1(\Omega_h); u_h|_T \in P_1(T) \ \forall T \in \mathcal{T}_h \right\}, \tag{2.7}$$

$P_1(T) = \{p|_T; p \in P_1\}$, P_1 denotes the set of all linear functions and $\mathcal{L}_h$, f_h, $\mathcal{B}_h$, V_h are the discrete analogues of $\mathcal{L}$, $f, \mathcal{B}$, V, respectively. Both possibilities $U_h \subset U$ and $U_h \not\subset U$ are admissible. Let us suppose, that the *discrete problem* (2.4) – (2.6) has a unique solution u_h.

To measure how close is the approximate solution u_h to the exact solution u we define the *discretization error* as

$$e_h \equiv \|u - u_h\|_X, \tag{2.8}$$

where $\|\cdot\|_X$ is a suitable norm such that the expression $\|v\|_X$ has a sense $\forall v \in U \cup U_h$. (If $U_h \subset U$ we can put $\|\cdot\|_X \equiv \|\cdot\|_U$, where $\|\cdot\|_U$ is the norm in the space U.)

Our aim is, for a given tolerance $\omega > 0$, to compute the approximate solution satisfying

$$e_h \leq \omega. \tag{2.9}$$

In [9] we presented the necessary condition for the relation (2.9). We denote by $\mathcal{O}(U, U_h)$ the set of all operators from U to U_h, i.e.

$$\mathcal{O}(U, U_h) = \{\Pi, \Pi : w \in U \mapsto \Pi w \in U_h\}. \tag{2.10}$$

Let us consider the minimization problem: Find $\Pi_h \in \mathcal{O}(U, U_h)$ such that

$$\|w - \Pi_h w\|_X = \min_{w_h \in U_h} \|w - w_h\|_X \quad \forall w \in U \tag{2.11}$$

The existence of Π_h follows from the fact that U_h is a finite dimensional space. The operator Π_h may not be uniquely determined, its uniqueness depends on the choice of $\|\cdot\|_X$.

It is evident that for the approximate solution u_h of (2.4) – (2.6)

$$\|u - \Pi_h u\|_X \leq e_h. \tag{2.12}$$

Then the necessary condition to fulfill (2.9) is

$$\|u - \Pi_h u\|_X \leq \omega. \tag{2.13}$$

Under some assumption on u and putting $\|\cdot\|_X = \|\cdot\|_{L^\infty(\Omega)}$, we derived in [9] the adaptation of a given triangulation in this way so that the new triangulation satisfies (2.13). The adaptation algorithm is briefly described in the following section.

2.2 Optimal triangulation and its construction

Let $\mathcal{T}_h$ be a triangulation of Ω_h used for the numerical solution of BVP (2.1) – (2.3) and $u_h \in U_h$ the approximate solution given by (2.4) – (2.6). By σ_h we denote the set of all vertices of triangles from $\mathcal{T}_h$. We introduce the smoothing of u_h as a function $\tilde{u} \in C^2(\Omega)$ approximating u_h, for more detail see [6], [9]. Let $\boldsymbol{H}(P_i)$, $P_i \in \sigma_h$ be the Hess matrix of the function $\tilde{u}$ evaluated in the vertex P_i

$$\boldsymbol{H}(P_i) = \begin{pmatrix} \frac{\partial^2 \tilde{u}}{\partial x^2} & \frac{\partial^2 \tilde{u}}{\partial x \partial y} \\ \frac{\partial^2 \tilde{u}}{\partial y \partial x} & \frac{\partial^2 \tilde{u}}{\partial y^2} \end{pmatrix} (P_i), \qquad P_i \in \sigma_h. \tag{2.14}$$

As $\boldsymbol{H}(P_i)$ is symmetric, we decompose it in the following way:

$$\boldsymbol{H}(P_i) = R_i \begin{pmatrix} \lambda_{i1} & 0 \\ 0 & \lambda_{i2} \end{pmatrix} R_i^{-1}, \quad P_i \in \sigma_h, \tag{2.15}$$

where R_i are orthogonal matrixes. As matrices $\boldsymbol{H}(P_i)$ are generally not positive definite, we put

$$\hat{\boldsymbol{H}}(P_i) = R_i \begin{pmatrix} |\lambda_{i1}| & 0 \\ 0 & |\lambda_{i2}| \end{pmatrix} R_i^{-1}. \tag{2.16}$$

The matrices $\hat{\boldsymbol{H}}(P_i),\ P_i \in \sigma_h$ are symmetric positive definite. Furthermore we put

$$\boldsymbol{M}(P_i) = c\left[\boldsymbol{I} + \alpha(\|\hat{\boldsymbol{H}}(P_i)\|)\hat{\boldsymbol{H}}(P_i))\right] \quad P_i \in \sigma_h, \tag{2.17}$$

where $\boldsymbol{I}$ is a unit 2×2 matrix, $c > 0$ is a constant and $\alpha : \langle 0,\infty) \to \langle 0,\infty)$ is a function. In (2.17) we put $\|\hat{\boldsymbol{H}}\| = \max_{i,j=1,2}|\hat{h}_{ij}|$, where $\hat{h}_{ij},\ i,j = 1,2$ are the elements of $\hat{\boldsymbol{H}}$, see [9]. The matrixes $\boldsymbol{M}(P_i),\ P_i \in \sigma_h$ are symmetric positive definite.

Let $\{S_k,\ k\in K\}$ (K is an index set) be the set of all edges of $\mathcal{T}_h$. Then we put

$$\bar{\boldsymbol{M}}_k = \frac{1}{2}\left(\boldsymbol{M}(P_{k_1}) + \boldsymbol{M}(P_{k_2})\right), \tag{2.18}$$

where $P_{k_1}\in\sigma_h$ and $P_{k_2}\in\sigma_h$ are the initial and final nodes forming $S_k,\ k\in K$, respectively. We define the *norm* of the edge S_k *corresponding to* the matrix $\bar{\boldsymbol{M}}_k$ by

$$\|S_k\|_{\bar{\boldsymbol{M}}_k} \equiv \left((S_k)^T\bar{\boldsymbol{M}}_k S_k\right)^{1/2}, \tag{2.19}$$

where $(S_k)^T\bar{\boldsymbol{M}}_k S_k$ means the vector-matrix-vector product, see (2.23). Moreover we put

$$Q_{\mathcal{T}_h} = \frac{1}{\#\mathcal{T}_h}\sum_{k\in K}\left(\|S_k\|_{\bar{\boldsymbol{M}}_k} - \sqrt{3}\right)^2, \tag{2.20}$$

where $\#\mathcal{T}_h$ is a the number of edges of $\mathcal{T}_h$. We call the quantity $Q_{\mathcal{T}_h}$ *the quality parameter* of $\mathcal{T}_h$. We say that the triangulation $\mathcal{T}_h^{\mathrm{opt}}$ is **optimal** if

$$Q_{\mathcal{T}_h^{\mathrm{opt}}} = \min Q_{\mathcal{T}_h}, \tag{2.21}$$

where the minimum is taken over all triangulations of Ω_h.

To construct the suitable triangulation we use an iterative algorithm consisting of the local operations: adding a node at the center of an edge, removing an edge, swapping the diagonal of the quadrilateral formed by any pair of adjacent elements and moving nodes. The mesh adaptation algorithm **minimizes the quality parameter** $Q_{\mathcal{T}_h}$. For more detail see [6] and [9].

The extension to the system (i.e. the solution of considered BVP is a vector function $\boldsymbol{u} : \Omega \to I\!R^N,\ \boldsymbol{u} = (u_1, u_2, \ldots, u_N)$) is straightforward. We chose one component of $\boldsymbol{u}$ as a *leading component* for the computation of $\boldsymbol{H}$ in (2.14) and the presented technique is applied.

2.3 Geometrical interpretation of AMA

In this section we illustrate the geometrical properties of the optimal triangulation generated by AMA technique described in the previous section. We roughly deduce from (2.21) – (2.20), that AMA adapts a given triangulation in such a way, so that the norm $\|S_k\|_{\bar{\boldsymbol{M}}_k}$ of each edge S_k is as close as possible to $\sqrt{3}$.

Let $S_k,\ k\in K$ be an edge of $\mathcal{T}_k$ and $\bar{\boldsymbol{M}}_k$ its corresponding symmetric positive definite matrix given by (2.18). We denote by $\boldsymbol{x}^k = (x_1^k, x_2^k)$ the center of edge S_k and the elements of $\bar{\boldsymbol{M}}_k$ as

$$\bar{\boldsymbol{M}}_k = \begin{pmatrix} a_k & b_k \\ b_k & c_k \end{pmatrix}. \tag{2.22}$$

Then the algebraic equation

$$
\begin{aligned}
&\left(x_1 - x_1^k, x_2 - x_2^k\right) \begin{pmatrix} a_k & b_k \\ b_k & c_k \end{pmatrix} \begin{pmatrix} x_1 - x_1^k \\ x_2 - x_2^k \end{pmatrix} = \\
= \quad & a_k (x_1 - x_1^k)^2 + 2b_k (x_1 - x_1^k)(x_2 - x_2^k) + c_k (x_2 - x_2^k)^2 = \frac{3}{4}, \\
& (x_1, x_2) \in I\!R^2
\end{aligned}
\tag{2.23}
$$

defines en ellipse ε_k with the centre $\boldsymbol{x}^k$. The relation between the triplet $(S_k, \bar{\boldsymbol{M}}_k, \varepsilon_k)$ and the optimal triangulation is given by the following lemma.

Lemma 1 *Let S_k, $k \in K$ be an edge of $\mathcal{T}_k$, $\boldsymbol{x}^k = (x_1^k, x_2^k)$ its center and $\bar{\boldsymbol{M}}_k$ its corresponding symmetric positive definite matrix given by* (2.18) *with matrix elements a_k, b_k, c_k in the form* (2.22)*. Let ε_k be the ellipse given by* (2.23)*. Let $\boldsymbol{x}^A, \boldsymbol{x}^B \in I\!R^2$ by two point lying on ε_k such that $\boldsymbol{x}^k$ is the centre of the abscissa $\boldsymbol{x}^A\boldsymbol{x}^B$, (see Fig. 1). Then*

$$
\|\boldsymbol{x}^A\boldsymbol{x}^B\|_{\bar{\boldsymbol{M}}_k} = \sqrt{3}. \tag{2.24}
$$

Proof. If $\boldsymbol{x}^A = \left(x_1^A, x_2^A\right)$ lies on ε_k then its coordinates satisfy

$$
a_k \left(x_1^A - x_1^k\right)^2 + 2b_k \left(x_1^A - x_1^k\right)\left(x_2^A - x_2^k\right) + c_k \left(x_2^A - x_2^k\right)^2 = \frac{3}{4}. \tag{2.25}
$$

As $\boldsymbol{x}^B$ lies on ε_k an $\boldsymbol{x}^k$ is the center of the abscissa $\boldsymbol{x}^A\boldsymbol{x}^B$ then

$$
\boldsymbol{x}^B = \boldsymbol{x}^k + (\boldsymbol{x}^k - \boldsymbol{x}^A) \tag{2.26}
$$

and then the coordinates satisfy

$$
x_i^B = 2x_i^k - x_i^A, \quad i = 1, 2. \tag{2.27}
$$

We compute the norm of $\boldsymbol{x}^A\boldsymbol{x}^B$ corresponding to $\bar{\boldsymbol{M}}_k$. From (2.19) we have

$$
\|\boldsymbol{x}^A\boldsymbol{x}^B\|^2_{\bar{\boldsymbol{M}}_k} = a_k \left(x_1^A - x_1^B\right)^2 + 2b_k \left(x_1^A - x_1^B\right)\left(x_2^A - x_2^B\right) + c_k \left(x_2^A - x_2^B\right)^2. \tag{2.28}
$$

Putting (2.27) in (2.28) and using (2.25) we have

$$
\begin{aligned}
\|\boldsymbol{x}^A\boldsymbol{x}^B\|^2_{\bar{\boldsymbol{M}}_k} \quad = \quad & a_k \left(x_1^A - (2x_1^k - x_1^A)\right)^2 + \\
& + 2b_k \left(x_1^A - (2x_1^k - x_1^A)\right)\left(x_2^A - (2x_2^k - x_2^A)\right) + \\
& + c_k \left(x_2^A - (2x_2^k - x_2^A)\right)^2 = \\
= \quad & 4\left[a_k \left(x_1^A - x_1^k\right)^2 + 2b_k \left(x_1^A - x_1^k\right)\left(x_2^A - x_2^k\right) + c_k \left(x_2^A - x_2^k\right)^2\right] = \\
= \quad & 4\frac{3}{4} = 3,
\end{aligned}
\tag{2.29}
$$

which proves the lemma. $\square$

It follows from Lemma 1, that AMA adapts $\mathcal{T}_h$ in this way, that the edge S_k is a chord of the ellipse ε_k going through its centre.

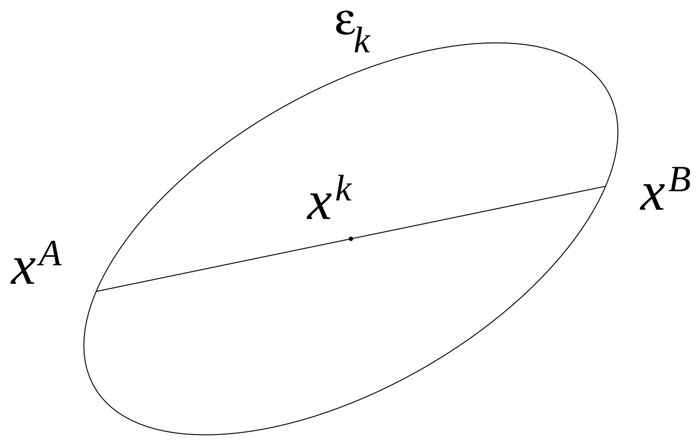

Figure 1: Example of the ellipse ε_k and two pairs of points $\boldsymbol{x}^A, \boldsymbol{x}^B$ and $\bar{\boldsymbol{x}}^A, \bar{\boldsymbol{x}}^B$

The relations (2.22) and (2.23) give that for any symmetric positive definite matrix $\bar{\boldsymbol{M}}_k$ there exists the ellipse ε_k. As $\bar{\boldsymbol{M}}_k$ is symmetric we decompose it in the following way

$$\begin{aligned} \bar{\boldsymbol{M}}_k &\equiv \begin{pmatrix} a_k & b_k \\ b_k & c_k \end{pmatrix} = R^T \Lambda R = \\ &= \begin{pmatrix} \cos\theta & \sin\theta \\ -\sin\theta & \cos\theta \end{pmatrix} \begin{pmatrix} \lambda_1 & 0 \\ 0 & \lambda_2 \end{pmatrix} \begin{pmatrix} \cos\theta & -\sin\theta \\ \sin\theta & \cos\theta \end{pmatrix}, \end{aligned} \tag{2.30}$$

where λ_1, λ_2 are the eigenvalues of $\bar{\boldsymbol{M}}_k$ and $\theta \in [0, 2\pi)$. We showed in [6] that the ellipse ε_k has the axes lengths $r_1 = 1/\sqrt{\lambda_1}, r_2 = 1/\sqrt{\lambda_2}$ and the angle between the axis x_1 and the major axis of ε_k is θ, see Fig. 2.

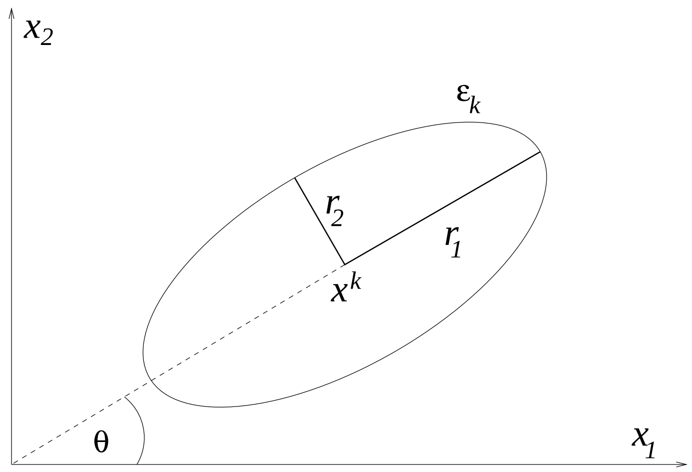

Figure 2: The ellipse ε_k with axes lengths $r_1 = 1/\sqrt{\lambda_1}, r_2 = 1/\sqrt{\lambda_2}$ and the angle θ

On the other hand to any triplet (r_1, r_2, θ), (r_1 and r_2 are real positive numbers and $\theta \in [0, 2\pi)$) defining the ellipse ε_k, there exists a matrix $\boldsymbol{M}_k$ given by (2.30). This properties will be important in the Section 4, where we require the satisfaction not only the necessary condition (2.13) but also other conditions following from physical aspects of viscous compressible flow.

3 Computation of viscous compressible flow

We present the mathematical model describing the motion of viscous compressible flow in bounded plane domain and the method for its numerical solution, which was intensively investigated during last years.

3.1 Formulation of the problem

We consider gas flow in a space-time cylinder $Q_T = \Omega \times (0, T)$, where $\Omega \subset \mathbb{R}^2$ is a bounded domain representing the region occupied by the fluid and $T > 0$. The complete system of viscous compressible flow consisting of the continuity equation, Navier–Stokes equations and energy equation can be written in the form

$$\frac{\partial \boldsymbol{w}}{\partial t} + \sum_{s=1}^{2} \frac{\partial \boldsymbol{f}_s(\boldsymbol{w})}{\partial x_s} = \sum_{s=1}^{2} \frac{\partial \boldsymbol{R}_s(\boldsymbol{w}, \nabla \boldsymbol{w})}{\partial x_s} \quad \text{in } Q_T. \tag{3.1}$$

Here

$$\begin{aligned}
&\boldsymbol{w} = (w_1,\, w_2,\, w_3,\, w_4)^T = (\rho,\, \rho v_1,\, \rho v_2, e)^T, \\
&\boldsymbol{w} = \boldsymbol{w}(x,t), \quad \boldsymbol{x} \in \Omega,\ t \in (0,T), \\
&\boldsymbol{f}_i(\boldsymbol{w}) = (\rho v_i,\, \rho v_i v_1 + \delta_{i1} p,\, \rho v_i v_2 + \delta_{i2} p,\, (e+p)\, v_i)^T, \\
&\boldsymbol{R}_i(\boldsymbol{w}, \nabla \boldsymbol{w}) = \left(0,\, \tau_{i1},\, \tau_{i2},\, \tau_{i1} v_1 + \tau_{i2} v_2 + \frac{\gamma}{Re\ Pr} \frac{\partial \theta}{\partial x_i}\right)^T, \\
&\tau_{ij} = \frac{1}{Re} \left[\left(\frac{\partial v_i}{\partial x_j} + \frac{\partial v_j}{\partial x_i} \right) - \frac{2}{3} \mathrm{div} \boldsymbol{v}\, \delta_{ij} \right], \quad i, j = 1, 2.
\end{aligned} \tag{3.2}$$

From thermodynamics we have

$$p = (\gamma - 1)\,(e - \rho |\boldsymbol{v}|^2/2), \quad e = \rho(\theta + |\boldsymbol{v}|^2/2). \tag{3.3}$$

We use the standard notation for dimensionless quantities: t – time, x_1, x_2 – Cartesian coordinates in $\mathbb{R}^2$, ρ – density, $\boldsymbol{v} = (v_1, v_2)$ – velocity vector with components v_i in the directions x_i, $i = 1, 2$, p – pressure, θ – absolute temperature, e – total energy, τ_{ij} – components of the viscous part of the stress tensor, δ_{ij} – Kronecker delta, $\gamma > 1$ – Poisson adiabatic constant, Re – Reynolds number, Pr – Prandtl number. We assume that $Pr = 0.72$. The functions $\boldsymbol{f}_i$, called inviscid (Euler) fluxes, are defined in the set $D = \{(w_1, \ldots, w_4) \in \mathbb{R}^4;\, w_1 > 0\}$. The viscous terms $\boldsymbol{R}_i$ are defined in $D \times \mathbb{R}^8$. (Due to physical reasons it is also suitable to require $p > 0$.)

System (3.1), (3.3) is equipped with the initial condition

$$\boldsymbol{w}(x, 0) = \boldsymbol{w}^0(x), \quad x \in \Omega \tag{3.4}$$

and boundary conditions. The boundary $\partial\Omega$ is formed by disjoint parts Γ_I, $\Gamma_O, \Gamma_W, \Gamma^+$ and Γ^-. On Γ_I, Γ_O and Γ_W, representing the inlet, outlet and impermeable profile, respectively, we prescribe the conditions

$$\begin{array}{llll} \text{(i)} & \rho = \rho^*, \quad v_i = v_i^*, \quad i = 1,\, 2, & \dfrac{\partial\theta}{\partial n} = \theta^* & \text{on } \Gamma_I, \\ \text{(ii)} & v_i = 0, \quad i = 1,\, 2, & \dfrac{\partial\theta}{\partial n} = 0 & \text{on } \Gamma_W, \\ \text{(iii)} & \displaystyle\sum_{i=1}^{2} \tau_{ij} n_i = 0, \quad j = 1,\, 2, & \dfrac{\partial\theta}{\partial n} = 0 & \text{on } \Gamma_O. \end{array} \tag{3.5}$$

Here $\partial/\partial n$ denotes the derivative in the direction of unit outer normal $\boldsymbol{n} = (n_1, n_2)^T$ to $\partial\Omega$; $\boldsymbol{w}^0$, ρ^*, v_i^* and θ^* are given functions. Moreover, on the artificial arcs Γ^- and Γ^+ we prescribe the periodicity boundary.

Let us note that equations (3.1) and (3.3) are of hyperbolic-parabolic type and that nothing is known about the existence and uniqueness of the solution of problem (3.1), and (3.3) – (3.5).

3.2 Numerical scheme

We carry out the discretization of the system (3.1), (3.3) with the use of the combination of finite volume and finite element methods. Let Ω_h be a polygonal approximation of the domain Ω. By $\mathcal{T}_h$ we denote a triangulation of Ω_h with standard properties for finite element method. By $\mathcal{S}_h$ we denote the set of all sides of all triangles $T \in \mathcal{T}_h$. We introduce a numbering of triangles $T \in \mathcal{T}_h$ and their sides $S \in \mathcal{S}_h$ in such a way that

$$\mathcal{T}_h = \{T_j;\ j \in J\}, \qquad \mathcal{S}_h = \{S_k;\ k \in K\}, \tag{3.6}$$

where J and K are suitable index sets. By Q_k we denote the centre of a side $S_k \in \mathcal{S}_h$ and put $I\!P_h = \{Q_k;\ k \in K\}$. Moreover, we set

$$K^\circ = \{i \in K;\ Q_i \in \Omega_h\}. \tag{3.7}$$

Now let us construct the *barycentric mesh* $\mathcal{D}_h = \{D_i; i \in K\}$ over the basic mesh $\mathcal{T}_h$. The *barycentric finite volume* D_i is a closed polygon defined in the following way: We join the barycentre of every triangle $T \in \mathcal{T}_h$ with its vertices. Then around the side S_i, $i \in K^\circ$, we obtain a closed quadrilateral containing S_i. If $S_j \subset \partial\Omega_h$ is a side with vertices P_1, P_2 of a triangle $T \in \mathcal{T}_h$ adjacent to $\partial\Omega_h$, then we denote by D_j the triangle with the sides S_j and segments connecting the barycentre of T with P_1 and P_2, see Fig. 3 and Fig. 4.

If $D_i \neq D_j$ and the set $\partial D_i \cap \partial D_j$ contains more than one point, we call D_i and D_j *neighbours* and set $\Gamma_{ij} = \partial D_i \cap \partial D_j$ (= a common side of D_i and D_j). Further, we define the set $s(i) = \{j \in J;\ D_j \text{ is a neighbour of } D_i\}$. If $Q_i \in \partial\Omega_h$, then we set $S(i) = s(i) \cup \{-1\}$ and $\Gamma_{i,-1} = S_i \subset \partial\Omega_h$, otherwise (for $i \in K^\circ$) we put $S(i) = s(i)$.

Let us consider a partition $0 = t_0 < t_1 < \ldots$ of the interval $(0, T)$ and set $\tau_k = t_{k+1} - t_k$ for $k = 0, 1, \ldots$. We denote by l_{ij} length of the segment Γ_{ij} and by $\boldsymbol{n}_{ij} = (n_{ij1}, n_{ij2})$ = unit outer normal to ∂D_i on Γ_{ij} (i.e., $\boldsymbol{n}_{ij}$ points from D_i to D_j).

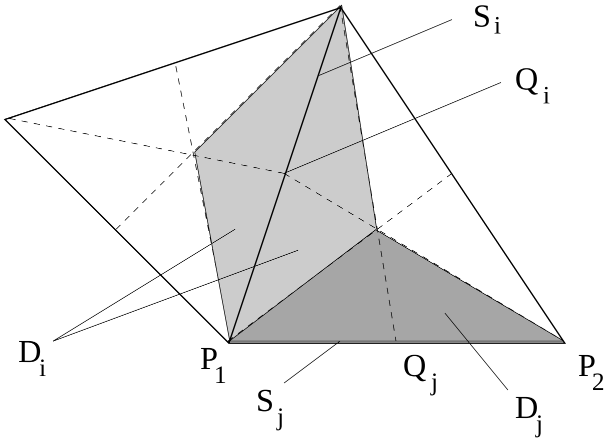

Figure 3: Barycentric finite volumes, $D_i, D_j \in \mathcal{D}_h,\ Q_i, Q_j \in I\!P_h,\ S_i, S_j \in \mathcal{S}_h,\ S_j \subset \partial\Omega_h$

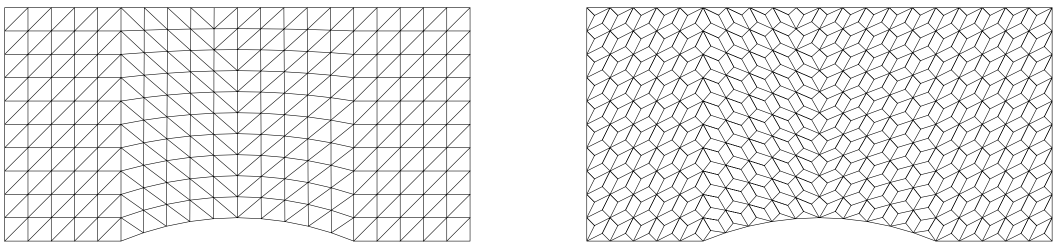

Figure 4: Triangular mesh and the associated barycentric finite volume mesh

Let us define the following space over the grid $\mathcal{T}_h$:

$$X_h = \left\{ v_h \in L^2(\Omega_h); v_h|_T \text{ is linear } \forall T \in \mathcal{T}_h, v_h \text{ is continuous at } Q_k \ \forall k \in K \right\}. \tag{3.8}$$

We use *nonconforming piecewise linear finite elements.* This means that the components of the state vector are approximated by functions from the finite dimensional space X_h defined in (3.8). Further, we set $\boldsymbol{X}_h = [X_h]^4$ and

$$\begin{array}{llcl} \text{a)} & \boldsymbol{V}_h & = & \{\varphi_h = (\varphi_1, \varphi_2, \varphi_3, \varphi_4) \in \boldsymbol{X}_h,\ \varphi_i(Q_j) = 0 \text{ for midpoints } Q_j \text{ lying} \\ & & & \text{on the part of } \partial\Omega_h \text{ where } w_i \text{ satisfies the Dirichlet condition} \\ & & & \text{and } \varphi_h \text{ satisfies periodicity condition}\}, \\ \text{b)} & \boldsymbol{W}_h & = & \{w_h \in \boldsymbol{X}_h; \text{ its components satisfy the Dirichlet boundary} \\ & & & \text{conditions following from (3.5) and periodicity condition}\}. \end{array}$$

Multiplying (3.1) considered on time level t_k by any $\varphi_h \in \boldsymbol{V}_h$, integrating over Ω_h, using Green's theorem, taking into account the boundary conditions (3.5) and the periodicity conditions for w, φ_h and for the derivatives of w, we obtain the following integral identity:

$$\int_{\Omega_h} \frac{\partial \boldsymbol{w}}{\partial t} \varphi_h \mathrm{d}\boldsymbol{x} + \int_{\Omega_h} \sum_{s=1}^{2} \frac{\partial \boldsymbol{f}_s(\boldsymbol{w})}{\partial x_s} \varphi_h \mathrm{d}\boldsymbol{x} + \int_{\Omega_h} \sum_{s=1}^{2} \boldsymbol{R}_s(\boldsymbol{w}, \nabla \boldsymbol{w}) \frac{\partial \varphi_h}{\partial x_s} \mathrm{d}\boldsymbol{x} = 0. \tag{3.9}$$

We approximate the convective terms with fluxes $\boldsymbol{f}_s$ by a form b_h with the aid of the finite volume approach. We define the form

$$b_h(\boldsymbol{u}, \boldsymbol{v}) = \sum_{i \in J} \boldsymbol{v}(Q_i) \sum_{j \in S(i)} H\left(\boldsymbol{u}(Q_i), \boldsymbol{u}(Q_j), \boldsymbol{n}_{ij}\right) \ell_{ij}, \ \ \boldsymbol{u}, \boldsymbol{v} \in \boldsymbol{X}_h, \tag{3.10}$$

which approximates the term

$$\int_{\Omega} \sum_{s=1}^{2} \frac{\partial \boldsymbol{f}_s(\boldsymbol{u})}{\partial x_s} \boldsymbol{v} \ \mathrm{d}\boldsymbol{x}. \tag{3.11}$$

The function H is called a *numerical flux*. As H we use here the well-known *Osher-Solomon numerical flux* (cf. [11], [12]). We define the form $a_h(\boldsymbol{w}_h^k, \varphi_h)$, which approximates the viscous terms of

$$\int_{\Omega_h} \sum_{s=1}^{2} \boldsymbol{R}_s(\boldsymbol{w}_h^k,\ \nabla \boldsymbol{w}_h^k) \frac{\partial \varphi_h}{\partial x_s} \, \mathrm{d}\boldsymbol{x} \tag{3.12}$$

by a standard nonconforming piecewise linear finite element approach [10], [14]. Now approximating the time derivative by a forward difference, (3.10) and evaluating the integrals with the aid of the quadrature formula using midpoints of sides as integration points we arrive at the following scheme for the calculation of an approximate solution $\boldsymbol{w}_h^{k+1}$ on the $(k+1)$-st time level:

$$\begin{array}{ll} \text{a)} & \boldsymbol{w}_h^{k+1} \in \boldsymbol{W}_h, \\ \text{b)} & \displaystyle\int_{\Omega_h} \boldsymbol{w}_h^{k+1} \varphi_h \, \mathrm{d}\boldsymbol{x} = \int_{\Omega_h} \boldsymbol{w}_h^k \, \varphi_h \, \mathrm{d}\boldsymbol{x} - \tau_k \{ b_h(\boldsymbol{w}_h^k, \varphi_h) + a_h(\boldsymbol{w}_h^k, \varphi_h) \} \quad \forall \varphi_h \in \boldsymbol{V}_h. \end{array} \tag{3.13}$$

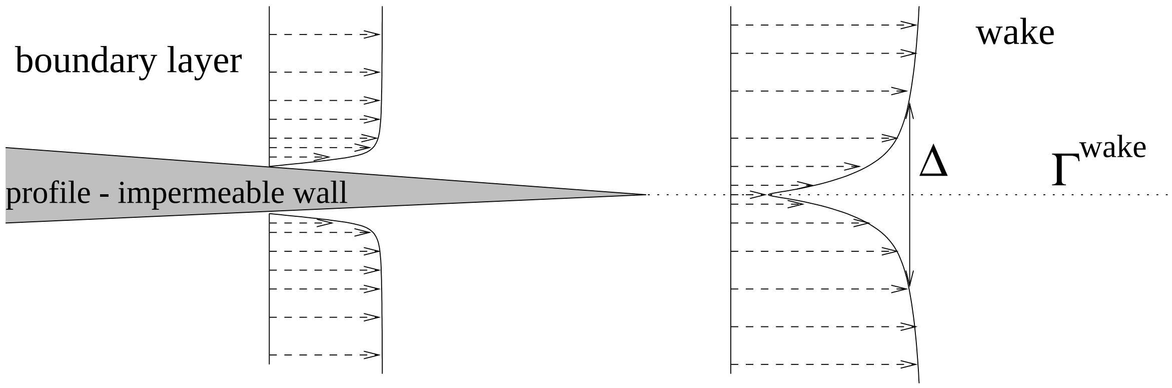

Figure 5: Example of Mach number flow field in a boundary layer and in a wake, the wake line $\Gamma^{\rm wake}$ and the width of the wake Δ

From (3.13) we see that the used scheme is fully explicit. The reason is its simple algorithmization. However, its application is conditioned by the use of a suitable *stability condition*. For more details see [8].

The convergence and the error estimates of the scheme (3.13) were done in [1] and [8] for scalar nonlinear convection diffusion equation, respectively.

4 AMA for viscous flow simulation

The application of AMA technique for the computation of inviscid transonic flow (i.e. $\boldsymbol{R}_i = 0,\ i = 1,2$ in (3.1)) was performed with success in [6], where the density ρ was chosen as the leading component of the state vector $\boldsymbol{w}$. This choice seems to be suitable because the triangulation was adapted along discontinuities (shock waves) and they were numerically captured with high accuracy.

Next possibility is to use the local Mach number $M = |\boldsymbol{v}|/\sqrt{\gamma p/\rho}$ as the leading component. The choice of M gives for inviscid flow similar results as for the density, because in subdomains $\Omega^s \subset \Omega$, where the components of $\boldsymbol{w}$ are smooth, the flow is isentropic and the density ρ is the function of M. On the other hand both ρ and M are discontinuous on the shock waves $(\Omega \setminus \Omega^s)$. The choice M as the leading component is more suitable for viscous flow simulation [4] because the velocity (and then Mach number) is essentially smaller in boundary layers and wakes than in the external flow and then the high gradient of Mach number will be detected by AMA. The Mach number flow field is viewed in Fig. 5.

The numerical examples show that the simple use of M as a leading component do not give satisfactory results for high speed flow with a small viscosity, because boundary layers and wakes are not satisfactory captured. Therefore an additional requirement has to be added to the mesh adaptation algorithm.

4.1 Boundary layer

At first we focus on the capturing of boundary layer. We present its physical properties, namely the dependence of the boundary thickness on the Reynolds number. Then we include

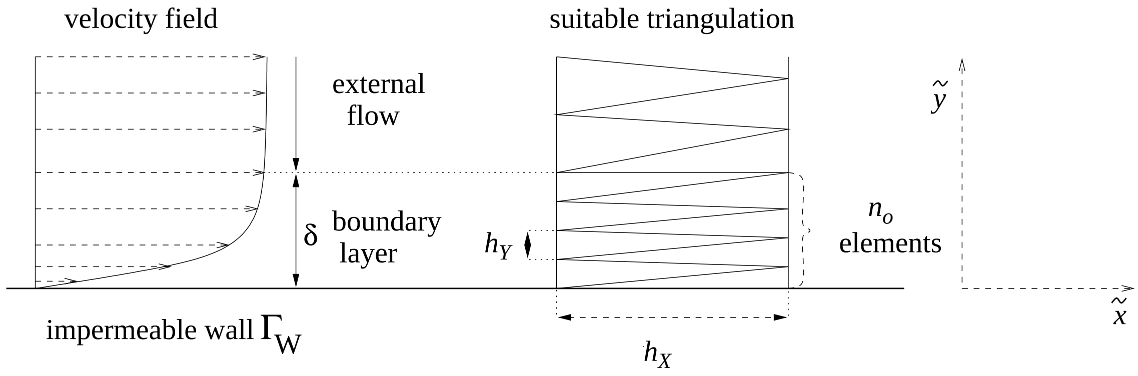

Figure 6: Illustration of the boundary layer with thickness δ and the sketch of a suitable triangulation with $n_0 = 4$

this property into AMA method.

4.1.1 Numerical capturing of boundary layer

Let us introduce a local coordinate system $\tilde{x}, \tilde{y}$ at the point lying on the impermeable wall Γ_W, where the condition (3.5ii) ($\boldsymbol{v} = 0$) is prescribed. The axis $\tilde{x}$ is the tangent to Γ_W and $\tilde{y}$ is perpendicular to Γ_W. It is known fact that the velocity does not change very much in the direction $\tilde{x}$ whereas the dependency of the velocity with respect to $\tilde{y}$ is very high. To capture precisely the boundary layer we have to generate a suitable triangulation along Γ_W, Fig. 6. We denote by h_X and h_Y the size of the triangle in the direction $\tilde{x}$ and $\tilde{y}$, respectively, see Fig. 6. The suitable triangulation for satisfactory capturing of a boundary layer is sketched at the middle part of Fig. 6. Triangles are thin and long and are alignment along Γ_W. The size h_Y has to be enough small to capture a boundary layer and it should successively increases with the distance from Γ_W. The size h_X has to be as high as possible so that the triangulation has as small as possible number of elements.

The thickness of the boundary layer δ depends on the flow viscosity according to the relation

$$\delta \approx \frac{1}{\sqrt{Re}}, \tag{4.1}$$

where Re is the Reynolds number. Then to well simulate the boundary layer we put

$$h_Y(0) = \frac{n_0}{\sqrt{Re}}, \tag{4.2}$$

where $n_0 > 1$ is a suitable constant and its meaning is viewed in Fig. 6. Numerical tests lead us to propose the value $n_0 \in \langle 3, 10 \rangle$. For triangles laying at the distance r_y from Γ_W we put

$$h_Y(r_y) = \frac{n_0}{\sqrt{Re}} + c_y^B r_y, \tag{4.3}$$

where c_y^B is a suitable constant.

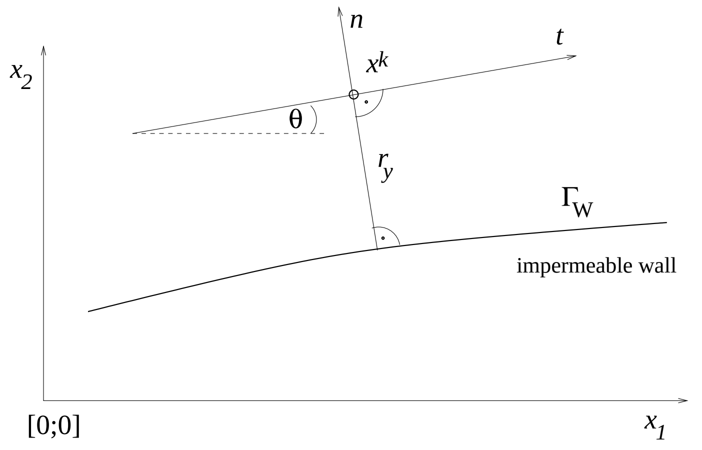

Figure 7: Construction of matrix $\boldsymbol{M}$ for boundary layer

On the other hand the size h_X of the triangle in the direction parallel with Γ_W is restricted only by *the minimal angle condition* required e.q. for FEM. Therefore we put

$$h_X = c_\alpha^B h_Y \tan \alpha_0, \tag{4.4}$$

where α_0 is the given minimal angle value and $0 < c_\alpha^B < 1$ is an "security" constant.

The relations (4.2) and (4.4) guarantee the sufficiently precise capturing of a boundary layer.

4.1.2 Boundary layer in the context of AMA

The previous consideration will be formulated in terms of AMA. Let $\boldsymbol{x}^k \in I\!R^2$ be a point in the vicinity of fixed wall and $\boldsymbol{n}$ denotes the normal from $\boldsymbol{x}^k$ to this wall. We denote by θ the angle between the axis x_1 and the tangent $\boldsymbol{t}$ and by r_y the distance of $\boldsymbol{x}^k$ to Γ_W, see Fig. 7.

According (4.4) and (4.3), it is suitable require that the length edge in the direction $\boldsymbol{n}$ and $\boldsymbol{t}$ are h_X and h_Y, respectively. Then using results from Section 2.3, we define to the point $\boldsymbol{x}^k$ the matrix

$$\boldsymbol{M}^B(\boldsymbol{x}_k) = \begin{pmatrix} \cos\theta & \sin\theta \\ -\sin\theta & \cos\theta \end{pmatrix} \begin{pmatrix} \frac{1}{h_X^2} & 0 \\ 0 & \frac{1}{h_Y^2} \end{pmatrix} \begin{pmatrix} \cos\theta & -\sin\theta \\ \sin\theta & \cos\theta \end{pmatrix}, \tag{4.5}$$

where θ is the angle between direction parallel with the wall and the axis x (see Fig. 7) and h_X and h_Y are given by (4.4) and (4.3), respectively. To the matrix $\boldsymbol{M}^B(\boldsymbol{x}^k)$ there exists an ellipse ε_k^B according (2.23) and then the norms (corresponding to $\boldsymbol{M}^B(\boldsymbol{x}^k)$) of all chords of ε_k^B going through $\boldsymbol{x}^k$ are equal to $\sqrt{3}$. Moreover, the length of the chord going through $\boldsymbol{x}^k$ parallel with $\boldsymbol{t}$ and $\boldsymbol{n}$ is equal to h_X and h_Y, respectively, which corresponds with our imagination of suitable triangulation for capturing a boundary layer.

As it is mentioned in [9], it is suitable for the practical implementation to come to vertex associated matrices. We define $\boldsymbol{M}^B(P_i)$, $P_i \in \sigma_h$ in the same way as $\boldsymbol{M}^B(\boldsymbol{x}^k)$. We have for each point $P_i \in \sigma_h$ two matrixes $\boldsymbol{M}(P_i)$ (given by (2.17) checking the fulfilling the necessary condition (2.13) and $\boldsymbol{M}^B$ (given by (4.5) checking the relations (4.3) – (4.4)). To satisfy both of this condition we use the so-called *intersection of matrices*, see [5].

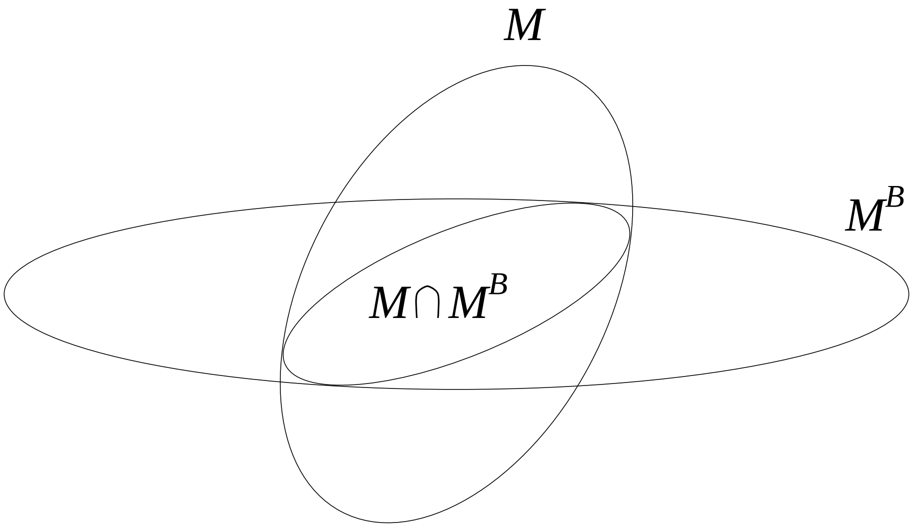

Figure 8: Intersection of two metrics.

4.1.3 Intersection of matrices

We say, that the matrix $\boldsymbol{M} \cap \boldsymbol{M}^B$ is the intersection of matrices $\boldsymbol{M}$ and $\boldsymbol{M}^B$, if the corresponding ellipse (Section 2.3) is the subset of ellipses corresponding to $\boldsymbol{M}$ and $\boldsymbol{M}^B$ and has the maximal possible area, see Fig. 8. We apply the transformation of coordinates to the system in which both $\boldsymbol{M}$ and $\boldsymbol{M}^B$ are diagonal, i.e. let $\boldsymbol{P}$ be a matrix such that

$$\tilde{\boldsymbol{M}} = \boldsymbol{P}^T \boldsymbol{M} \boldsymbol{P} = \begin{pmatrix} \lambda_1 & 0 \\ 0 & \lambda_2 \end{pmatrix}, \qquad \tilde{\boldsymbol{M}}^B = \boldsymbol{P}^T \boldsymbol{M}^B \boldsymbol{P} = \begin{pmatrix} \mu_1 & 0 \\ 0 & \mu_2 \end{pmatrix}, \tag{4.6}$$

where $\boldsymbol{P}^T$ denotes the matrix transpose to $\boldsymbol{P}$. Then putting

$$(\boldsymbol{M}, \boldsymbol{M}^B) = (\boldsymbol{P}^{-1})^T \begin{pmatrix} \max(\lambda_1, \mu_1) & 0 \\ 0 & \max(\lambda_2, \mu_2) \end{pmatrix} \boldsymbol{P}^{-1} \tag{4.7}$$

we obtain the desired matrix. Here $\boldsymbol{P}^{-1}$ means the inverse matrix to $\boldsymbol{P}$.

The matrix $\boldsymbol{P}$ is not defined uniquely and it can be set using the following relations. Let $\boldsymbol{M}$ and $\boldsymbol{M}^B$ are written in the form

$$\boldsymbol{M} = \begin{pmatrix} a_1 & b_1 \\ b_1 & c_1 \end{pmatrix}, \qquad \boldsymbol{M}^B = \begin{pmatrix} a_2 & b_2 \\ b_2 & c_2 \end{pmatrix}, \tag{4.8}$$

where $a_i > 0, c_i > 0, a_i c_i > b_i^2,\ i = 1, 2$. Then the matrix $\boldsymbol{P}$ is given by

$$\boldsymbol{P} = \begin{pmatrix} p_1 & p_2 \\ p_3 & p_4 \end{pmatrix} \tag{4.9}$$

with components given for example by the following relations

$$
\begin{array}{ll}
\textbf{if} & \exists C > 0 \text{ such that } a_1 = Ca_2,\ b_1 = Cb_2,\ c_1 = Cc_2 \\
\textbf{then} & \\
& a_1 \neq -b_1 \quad \Rightarrow \quad \begin{array}{l} p_1 = -\frac{b_1+c_1}{a_1+b_1} \\ p_2 = 1 \\ p_3 = 1 \\ p_4 = 1 \end{array} \\
& \\
& a_1 = -b_1 \quad \Rightarrow \quad \begin{array}{l} p_1 = 1 \\ p_2 = 1 \\ p_3 = 1 \\ p_4 = -\frac{a_1+b_1}{b_1+c_1} \end{array} \\
\textbf{else} & \\
& \begin{array}{l} d = (a_1c_2 - a_2c_1)^2 - 4(a_1b_2 - b_1a_2)(b_1c_2 - c_1b_2) \\ p_2 = \frac{a_2c_1 - a_1c_2 - \sqrt{d}}{2(a_1b_2 - b_1a_2)} \\ p_1 = -\frac{b_2p_2 + c_2}{p_2a_2 + b_2} \\ p_3 = 1 \\ p_4 = 1 \end{array}
\end{array}
\tag{4.10}
$$

It can be proved that if does not exist C such that $a_1 = Ca_2,\ b_1 = Cb_2,\ c_1 = Cc_2$ then d from (4.10) is always nonnegative.

The application of the viscous correction is obvious. We use the AMA technique described in Section 2 but the matrix $\boldsymbol{M}(P_i)$ is replaced by the matrix $\boldsymbol{M}(P_i) \cap \boldsymbol{M}^B(P_i)$ for nodes in vicinity of Γ_W.

4.2 Wake

A viscous flow around a profile gives rise to a wake behind the trailing edge of the profile. Its flow field is viewed in Fig. 5. To satisfactory accurate capture a wake, it is necessary to adapt the triangulation behind the profile. We use a similar approach for nodes in vicinity of a wake as for them in vicinity of boundary layers. We define *the wake line* Γ^{wake} starting at the trailing edge and parallel with the flow field behind the profile, see Fig. 5. Its position is known a priori (e.q. for symmetric problems) or it is set a posteriori from the results computed on the previous level of adaptation. Similarly as for a boundary layer we introduce a local coordinate system $\tilde{x}, \tilde{y}$ at the point lying on Γ^{wake}. The axis $\tilde{x}$ and $\tilde{y}$ are parallel and perpendicular with Γ^{wake}, respectively. Instead of the relations (4.4) and (4.3) we define the following relations

$$h_Y(r_y) = \frac{n_0}{\sqrt{Re}} + c_y^W \max(0, r_y - \Delta/2), \tag{4.11}$$

$$h_X = c_\alpha^W h_Y \tan \alpha_0, \tag{4.12}$$

where Δ means the width of the wake (Fig. 5) and c_y^W and c_α^W are constants similar as c_y^B and c_α^B, respectively. The magnitude of Δ depends on the considered problem.

Then we define the matrix $\boldsymbol{M}^W$ similarly as in (4.5) and use the intersection of matrix $\boldsymbol{M} \cap \boldsymbol{M}^W$ from Section 4.1.3.

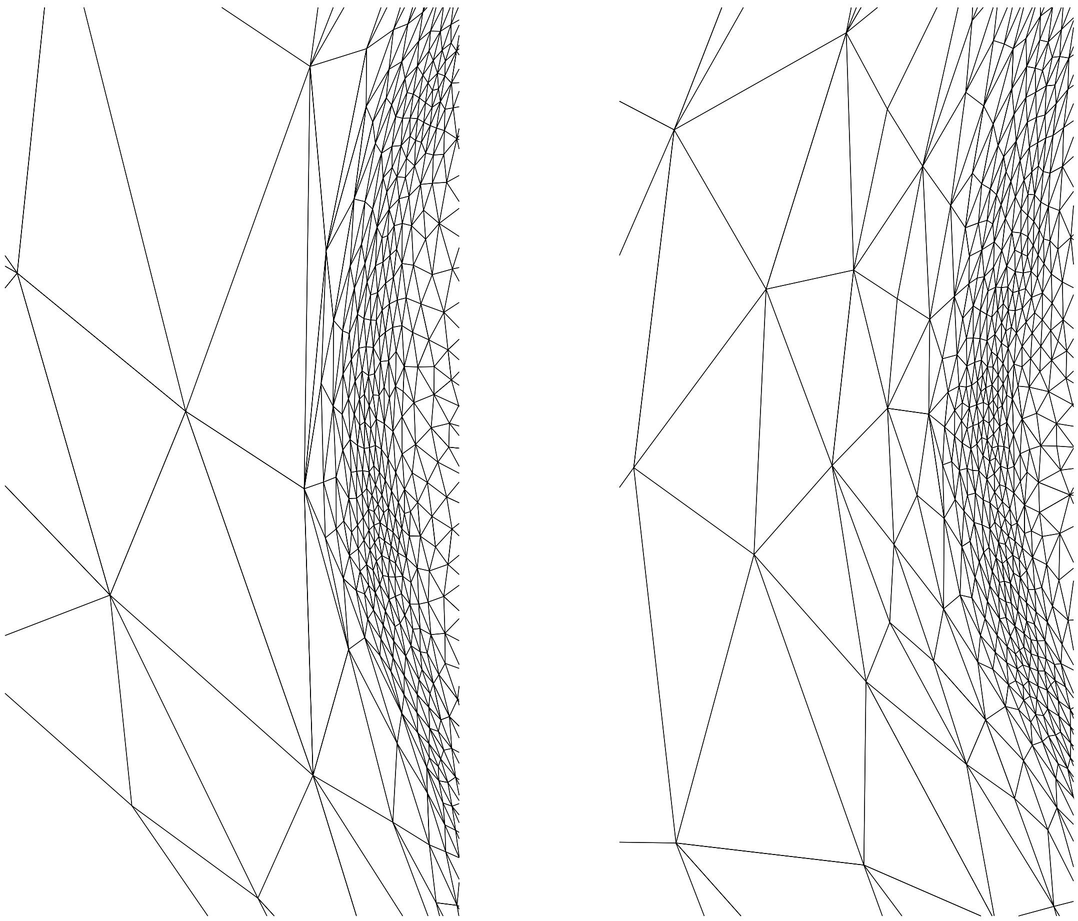

Figure 9: Mesh gradation control, triangulation without (left) and with (right) mesh gradation control

4.3 Mesh gradation control

The application of AMA technique presented in Sections 2, 4.1 and 4.2 can lead to triangulations with high gradation. It means that the sizes of neighbour triangles very differ, see Fig. 9 left. To high mesh gradation gives rise some troubles for different numerical solvers (FEM, FVM). The uncontrolled mesh gradation is caused by the fact, that matrixes $\boldsymbol{M}_i$ and $\boldsymbol{M}_j$ very differ for two nearby nodes P_i and P_j. Therefore our aim is to control the mesh gradation of the triangulation generated by AMA. It is illustrated in Fig. 9, where is shown the passage from the coarse part of the triangulation to the fine one (from left to right). The left and right figure are the triangulation generated without and with mesh gradation control, respectively. The use of mesh gradation control technique gives triangulations with better properties for numerical solution using FEM, but naturally the number of elements is higher.

We have applied two approaches from [2], the H-variation and H-shock. We present only the final relations, for more detail see [2]. Both H-variation and H-shock lead to similar grids.

4.3.1 H-variation

Let P_1P_2 be an edge of the triangulation $\mathcal{T}_h$ and $\boldsymbol{M}_{P_1}$ and $\boldsymbol{M}_{P_2}$ the matrices corresponding to nodes P_1 and P_2, respectively. Then we put

$$\begin{aligned} \boldsymbol{M}_{P_1} &:= \boldsymbol{M}_{P_1} \cap \boldsymbol{M}_{P_2}(1+\alpha\|P_1P_2\|_{\boldsymbol{M}_{P_1}})^{-2}, \quad \alpha > 0, \\ \boldsymbol{M}_{P_2} &:= \boldsymbol{M}_{P_2} \cap \boldsymbol{M}_{P_1}(1+\alpha\|P_1P_2\|_{\boldsymbol{M}_{P_2}})^{-2}, \end{aligned} \tag{4.13}$$

where $\|P_1P_2\|_{\boldsymbol{M}_{P_1}}$ and $\|P_1P_2\|_{\boldsymbol{M}_{P_2}}$ are the norms of the edge P_1P_2 corresponding to $\boldsymbol{M}_{P_1}$ and $\boldsymbol{M}_{P_2}$, respectively. The operator $\cap$ means the intersection of matrices, Section 4.1.3. We use the value $\alpha = 2$.

4.3.2 H-shock

Let P_1P_2 be an edge of the triangulation. We compute h_{P_1} and h_{P_2} the norm of the unit vector in the direction P_1P_2 corresponding to matrixes $\boldsymbol{M}_{P_1}$ and $\boldsymbol{M}_{P_2}$, respectively. Let $l_{P_1P_2}$ be the norm of P_1P_2 corresponding to matrix $\bar{\boldsymbol{M}}_{P_1P_2} = (\boldsymbol{M}_{P_1} + \boldsymbol{M}_{P_2})/2$. Then H-shock associated to the edge P_1P_2 is the value

$$c_{P_1P_2} = \left(\frac{h_{P_2}}{h_{P_1}}\right)^{1/l_{P_1P_2}}. \tag{4.14}$$

If $c_{P_1P_2} \geq \beta$ then we replace $\boldsymbol{M}_{P_2}$ by $\eta^{-2}\boldsymbol{M}_{P_2}$, where $\eta = \left(\frac{\beta}{c_{P_1P_2}}\right)^{l_{P_1P_2}}$. We use the value $\beta = 1.5$.

5 Numerical results

The described method (solver and mesh adaptation) was applied to the numerical simulation of flow past a turbine cascade shown in Figure 10. The goal was to obtain the steady state solution with the aid of the time stabilization for $t \to \infty$. The computational results are compared with a wind tunnel experiment (by courtesy of the Institute of Thermomechanics of the Czech Academy of Sciences in Prague, see [13]). The experiment and computations were performed for the following data: angle of attack $= 19^\circ\,18'$, inlet Mach number $= 0.32$, outlet Mach number $= 1.18$, $\gamma = 1.4$, Reynolds number $Re = 1.5 \cdot 10^6$, Prandtl number $Pr = 0.72$.

Figure 11 represents the wind tunnel interferogram showing density isolines. We compare the results achieved by combined FV - FE method (Section 3) using triangulations generated by AMA (Section 2) without and with viscous correction (Section 4). As the starting triangulation and numerical solution we use the results of inviscid flow simulation [7]. In Figure 12 and Figure 13 the final triangular mesh and the corresponding isolines of Mach number with zooms of trailing edge obtained with the aid of anisotropic mesh refinement with and without viscous correction are plotted, respectively. The viscous correction yields to the mesh refinement along profile and then the boundary layer is captured with high accuracy and the shock waves are not smeared as for the example without viscous mesh correction. Figure 14 shows the pressure distribution along the profile compared with the measurement. We see that a good agreement of computational results with experiment was achieved, if the viscous mesh correction is applied.

Acknowledgements

The research has been supported under the Grant No. 201/99/0267 and No. 201/00/D116 of the Czech Grant Agency and by the Grant MSM 113200007. The author gratefully acknowledges this supports.

References

[1] P. Angot, V. Dolejší, M. Feistauer, and J. Felcman. Analysis of a combined barycentric finite volume – nonconforming finite element method for nonlinear convection – diffusion problem. *Applications of Mathematics*, 43(4):263–310, 1998.

[2] H. Borouchaki, F. Hecht, and P. J. Frey. Mesh gradation control. In *Proceedings of 6th International Meshing Roundtable*, Park City, Utah, USA, 1997.

[3] P. G. Ciarlet. *The Finite Elements Method for Elliptic Problems.* North-Holland, Amsterodam, 1979.

[4] M. J. Castro Díaz, H. Borouchaki, P. L. George, F. Hecht, and B. Mohammadi. Anisotropic Adaptive Mesch Generation in Two Dimensions for CFD. In *Proceeding of ECCOMAS96 – Computational Fluid Dynamics, Paris*, pages 181–186, 1996.

[5] M. J. Castro Díaz, F. Hecht, and B. Mohammadi. New progress in anisotropic grid adaptation for inviscid and viscous flows simulations. In *Proceedings of the 4th Annual International Meshing Roundtable.* Sandia National Laboratories, 1995.

[6] V. Dolejší. Anisotropic mesh adaptation for finite volume and finite element methods on triangular meshes. *Computing and Visualisation in Science*, 1:165–178, 1998.

[7] V. Dolejší. *Combined Finite Volume – Finite Element Methods for Compressible Flow on Unstructured Meshes.* PhD thesis, Charles Univeristy Prague and Université Mediterannée Marseille, 1998.

[8] V. Dolejší, M. Feistauer, J. Felcman, and A. Kliková. Error estimates for barycentric finite volumes combined with nonconforming finite elements applied to nonlinear convection–diffusion problems. *Applications of Mathematics*, 1(1):(submitted), 2000.

[9] V. Dolejší and J. Felcman. Anisotropic mesh adaptation and its application for scalar diffusion equations. *Numerical Methods for Partial Differential Equations (submitted)*, 2000.

[10] M. Feistauer. *Mathematical Methods in Fluid Dynamics.* Longman Scientific & Technical,Harlow, 1993.

[11] M. Feistauer, J. Felcman, and M. Lukáčová. Combined finite elements–finite volume solution of compressible flow. *J. Comput. Appl. Math.*, 63:179–199, 1995.

[12] S. Osher and F. Solomon. Upwind difference schemes for hyperbolic systems of conservation laws. *Math. Comp.*, 38:339–374, 1982.

[13] M. Šťastný and P. Šafařík. Experimental analysis data on the transonic flow past a plane turbine. Technical report, ASME Paper 90-GT-313, New York, 1990.

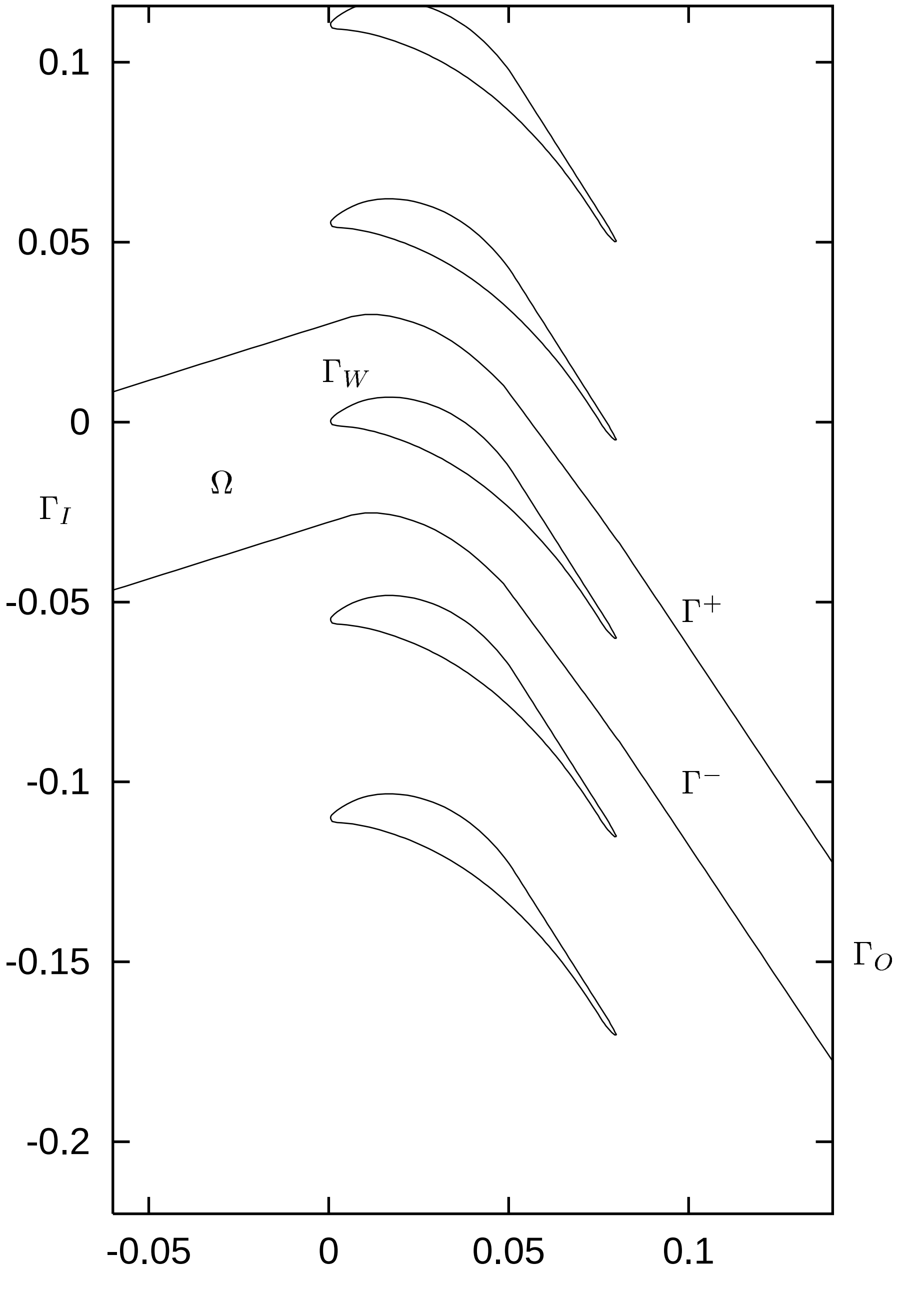

Figure 10: Cascade of profiles with the computational domain Ω and the boundary parts Γ_I, Γ_O, Γ_W and the artificial periodical cuts Γ^+ and Γ^-

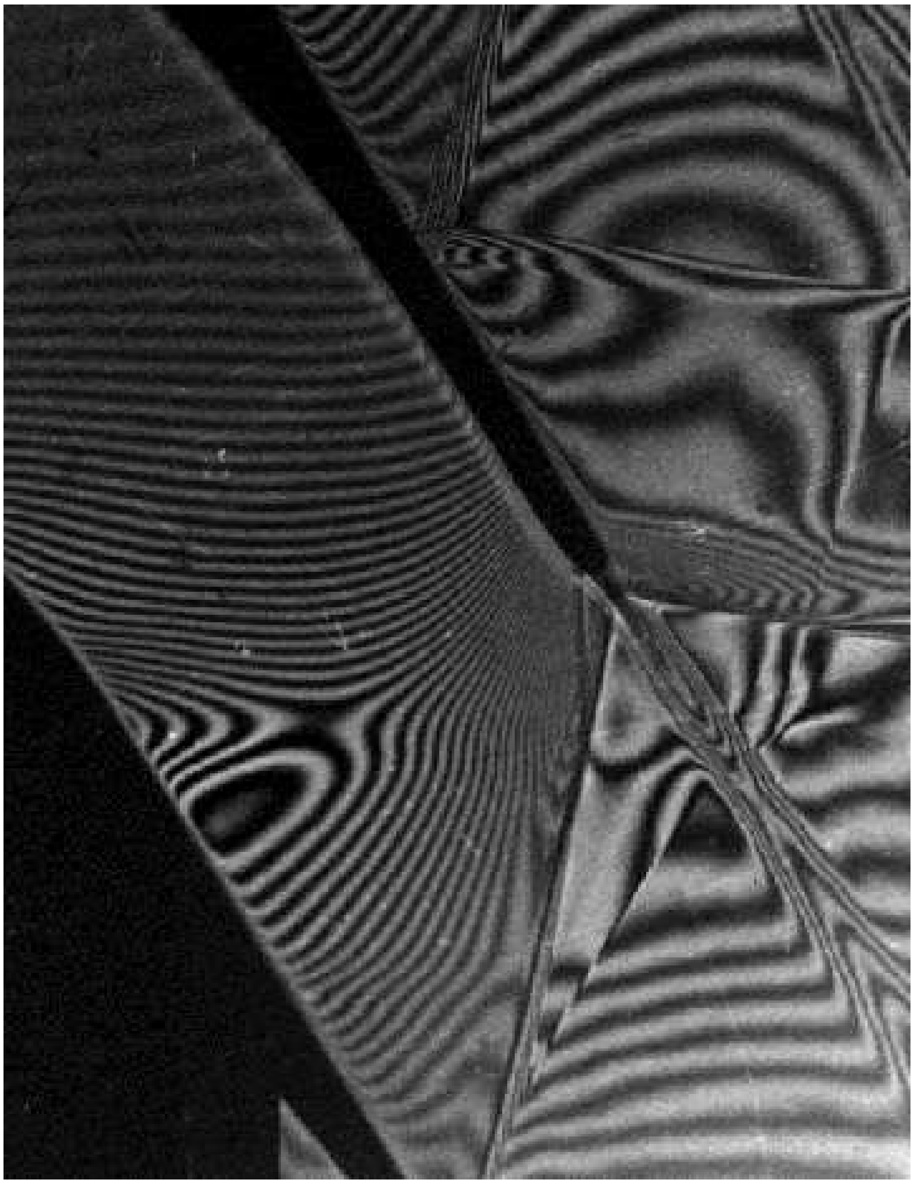

Figure 11: The wind tunnel interferogram showing density isolines (Courtesy of the Institute of Thermomechanics, Czech Academy of Science, Prague)

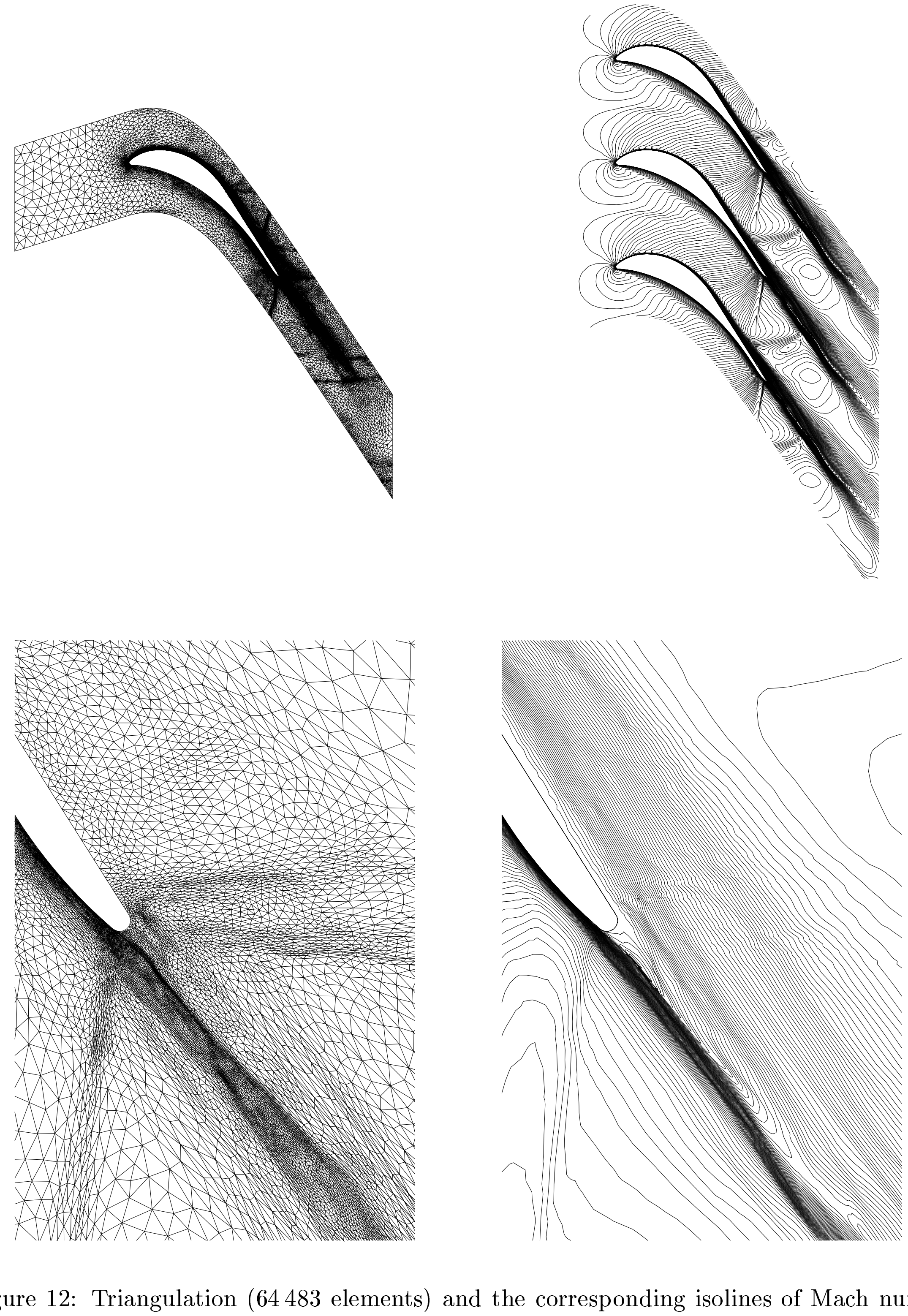

Figure 12: Triangulation (64 483 elements) and the corresponding isolines of Mach number with zoom achieved by AMA without viscous correction

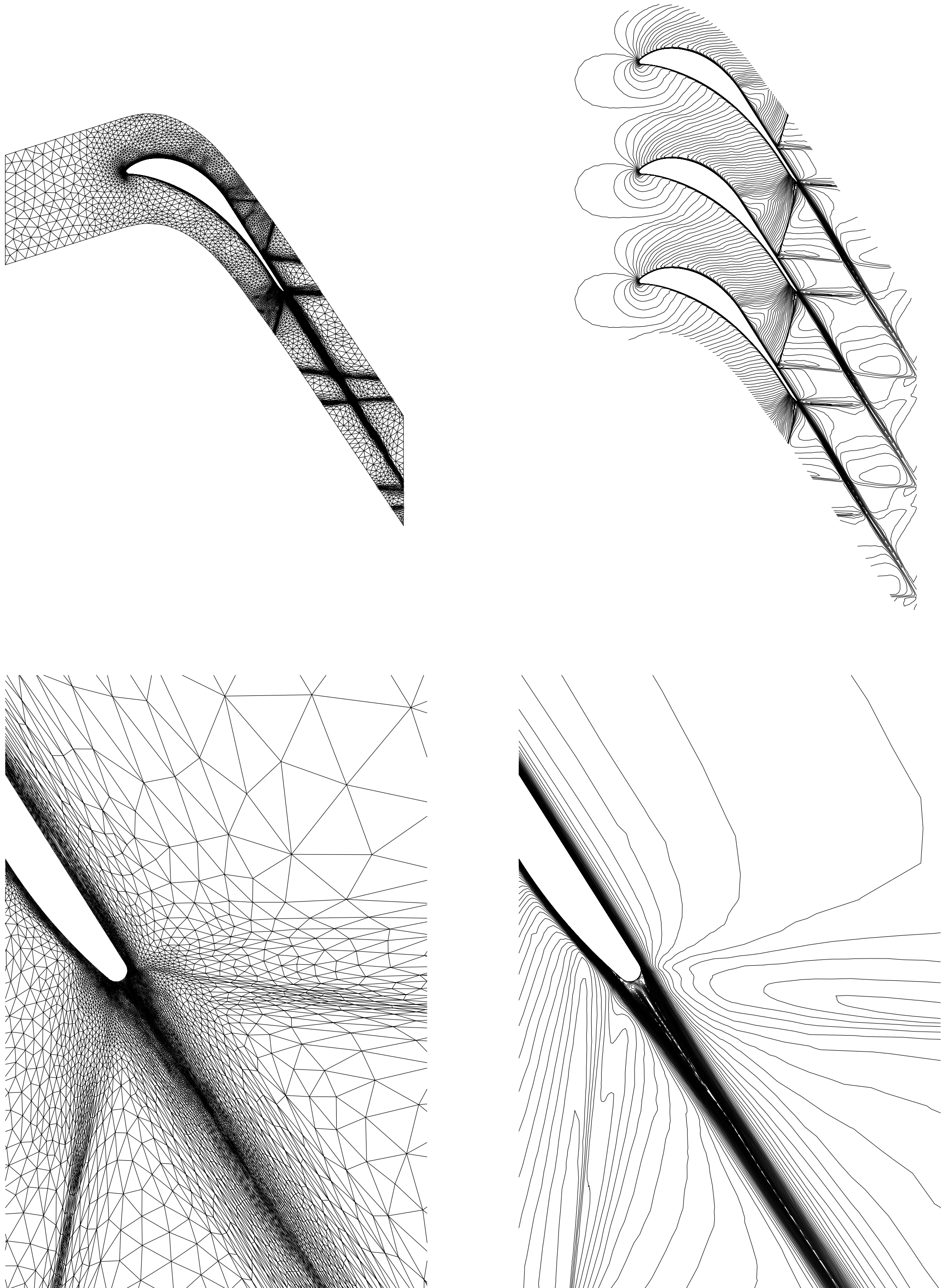

Figure 13: Triangulation (38 086 elements) and the corresponding isolines of Mach number with zoom achieved by AMA with viscous correction

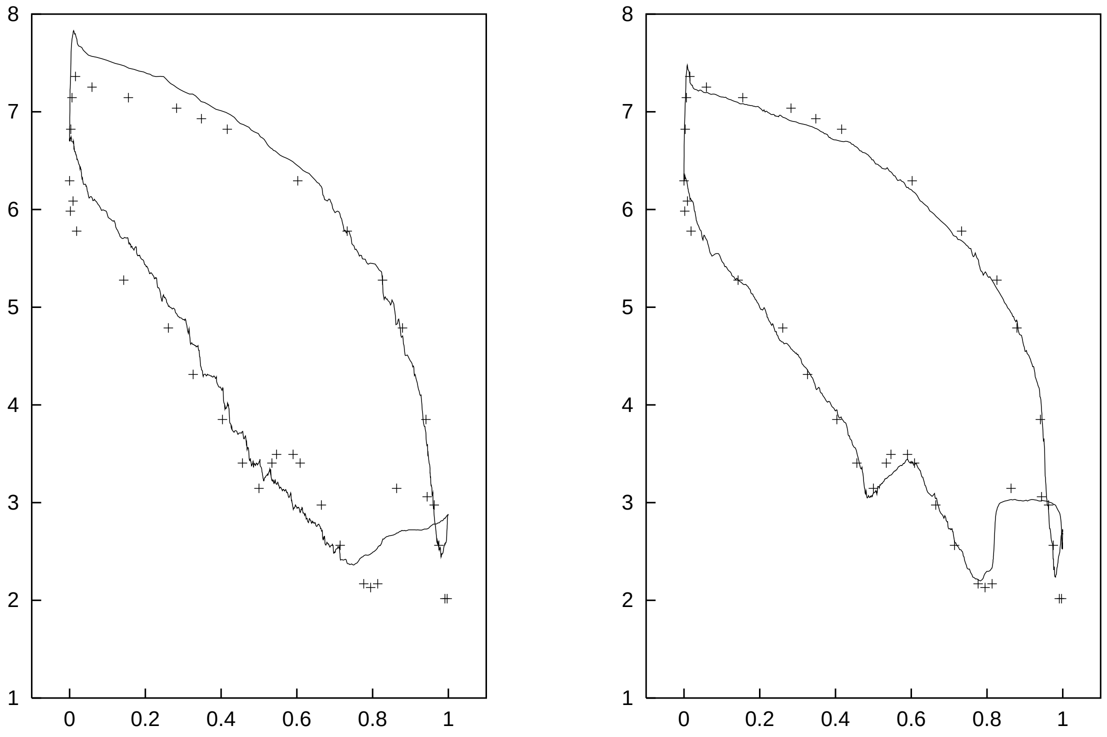

Figure 14: Distribution of the pressure (full line) in comparison with measurement (separated nodes) without (left) and with (right) AMA viscous correction

[14] R. Teman. *Navier – Stokes Equations.* North – Holland, Amsterodam – New York – Oxford, 1977.

List of preprints released in this series

All preprints available on http://www.karlin.mff.cuni.cz/ms-preprints/
E-mail contact to series administrator: knm-prep@karlin.mff.cuni.cz

[MATH-ALG-2001/1] J.Trlifaj: *Approximations and the little finitistic dimension of artinian rings* (30.01.2001)

[MATH-KMA-2001/42] Jakub Duda, Libor Vesely, Ludek Zajicek: *On D.C. functions and mappings* (31.01.2001)

[MATH-KMA-2001/43] W.D. Evans, Bohumir Opic, Lubos Pick: *Real interpolation with logarithmic functors* (31.01.2001)

[MATH-KMA-2001/44] Robert Cerny, Jan Maly: *Yet more counterexample to lower semicontinuity in Calculus of Variations* (14.02.2001)

[MATH-KMA-2001/45] Wolfgang Desch, Eva Fasanga, Jaroslav Milota, Wilhelm Schappacher: *Stress boundary value problem in linear viscoleasticity* (14.02.2001)

[MATH-KMA-2001/46] Ondrej Kalenda: *A new Banach space with Valdivia dual unit ball* (21.02.2001)

[MATH-KMA-2001/47] Petr Holicky, Roman Kotecky, Milos Zahradnik: *Phase diagram of horizontally invariant Gibbs states for lattice models* (27.02.2001)

[MATH-KMA-2001/48] Stanislav Hencl: *On the notions of absolute continuity for functions of several variables* (27.02.2001)

[MATH-KMA-2001/49] Jaroslav Lukes, Jan Maly, Ivan Netuka, Michal Smrcka, Jiri Spurny: *On approximation of affine Baire-one functions* (08.03.2001)